MECHANICAL BEHAVIOR OF QUATERNARY CONCRETE WITH MICRO/NANO SIO_2 ANALIZED BY ARTIFICIAL NEURAL NETWORKS AND SURFACE RESPONSE METHOD

Luis E Zapata-Orduz[1], Genock Portela[2], Marcelo Suárez[2], Brian H. Green[3]*

1: Escuela de Ingeniería Civil, Universidad Industrial de Santander, Cra 27 calle 9 Ciudad Universitaria UIS, Zip Code: 680002, Bucaramanga, Colombia.
2: Department of General Engineering, University of Puerto-Mayagüez Campus, PO BOX 9000, USA
3: Engineering and Materials Science Department, US Army Corps of Engineers, Vicksburg, MS, USA.

** e-mail: luisezap@uis.edu.co*

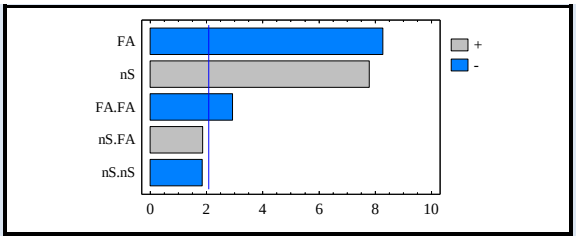

ABSTRACT

This paper presents experimental and computational findings related to the compressive strength of concrete containing nano-SiO_2, fly-ash, silica fume, and polycarboxylate-superplasticizer. At different days of aging, three central-composite experimental designs were performed to assess the role of the input variables. The statistical results indicated linear, interactive, and quadratic effects between the variables as well as mathematical lack-of-fit of the second-order. Hence, artificial neural networks (ANN) with multiple inputs were implemented to assist in understanding the complex nature of the systems. The results indicated that, by using ANN, the compressive strength of the systems could be modeled to improve the concrete´s performance acting in conjunction with results obtained from the statistical experimental designs. Sensitivity analyses on the ANN-simulations allowed for quantifying the influence of the multiple input variables and results were physically related to the mathematical lack-of-fit condition inherit in the statistical experimental designs.

Keywords: *compressive strength, nano-SiO_2, silica fume, fly ash, statistical design of experiments, artificial neural networks.*

COMPORTAMIENTO MECÁNICO DE MEZCLAS CUATERNARIAS DE CONCRETO CON MICRO/NANO SIO_2 ANALIZADAS EMPLEANDO REDES NEURONALES ARTIFICIALES Y EL MÉTODO DE SUPERFICIE DE RESPUESTA

RESUMEN

Este documento presenta los hallazgos experimentales y computacionales relacionados con la resistencia a la compresión del concreto adicionado con nano-SiO_2, cenizas volantes, humo de sílice y superplastificante del tipo policarboxilato. Se realizaron tres diseños experimentales centrales compuestos en diferentes días de maduración para evaluar el papel de las variables. Los resultados estadísticos indicaron efectos lineales, interactivos y cuadráticos entre las variables, así como falta de ajuste matemático de segundo orden en los diseños experimentales. Por lo tanto, se implementaron redes neuronales artificiales (ANN) con múltiples variables de entrada para ayudar a comprender la compleja naturaleza de los sistemas. Los resultados indicaron un excelente modelamiento de la resistencia a la compresión de los sistemas y mediante el uso de las ANN actuando en conjunto con los resultados obtenidos de los diseños experimentales se logró mejorar el entendimiento del concreto. Los análisis de sensibilidad en las simulaciones con las ANN permitieron cuantificar la influencia de las múltiples variables de entrada y los resultados se relacionaron con la condición matemática de falta de ajuste y explicaron físicamente con gran éxito los resultados de los diseños estadísticos experimentales que padecían dicha condición.

Palabras Clave: *resistencia a la compresión, nano-SiO_2, micro-sílice, ceniza volante, diseño estadístico de experimentos, redes neuronales artificiales.*

1. INTRODUCTION

Increasing employment of nano-modified, high-performance construction materials and systems, such as smart carbon nano-tubes, nano-titania, nano-calcium carbonate, and nano-alumina, is producing materials with higher strength, improved durability, and reduced environmental impact [1]. Specifically, among recent advances in the concrete industry seeking to make concrete more sustainable are the increasing use of binary, ternary, and even quaternary binders [2][3][4]. In effect, such modified cementitious materials result not only in the production of high strength concretes but also in more durable, sustainable, and economical concrete structures [5]. For instance, some years ago, the maximum compressive strength that could be obtained at the construction site was about 40 MPa [6], but today due to recent advancements in concrete technology and chemical and mineral admixtures, concrete with compressive strengths up to 100 MPa are commercially produced [7]. Also, according to the recent research, high strength concrete (HSC) could be considered as a special group of concrete materials due to incorporation of mineral and chemical admixtures so that the compressive strengths exceeds 70 MPa [8]. Nevertheless, in spite of this development in the concrete industry, concretes with compressive strengths of at least 40-60 MPa are still regarded as HSC. In fact, Jajal et al. [9] following the American Concrete Institute Committee ACI 363, defined HSC as the concrete that has a specific compressive strength of at least 41 MPa at 28 days. In this paper, 24 different mix designs with a water-to-binder (w/b) ratio of 0.35 were developed to obtain at least 41 MPa in compressive strength at 28 days by using Portland cement type I, Class F fly ash (FA), silica fume (SF), and nano-SiO_2 (nS) in plain, binary, ternary, and quaternary mixes. The compressive strength was studied at ages of 3, 7, 28, 56, and 90 days, and the analysis of the results were conducted by using both statistical and numerical computer tools, such as design of experiments (DOEs) and artificial neural network (ANN) models, respectively.

ANNs are a powerful tool and are extremely useful in situations for which the rules are either unknown or when response surfaces are highly complex. Hence, the use of ANNs is especially advantageous when traditional predictive mathematical models are not feasible [10][11][12][13]. However, the flexibility of ANN is linked to one of the most important of their disadvantages, i.e., they are unable to provide explanations and justifications for their answers [10]. In civil engineering, the ANN approach has been widely used to model and analyze a diversity of topics such as: soil behavior [14], torsion in reinforced concrete beams [15], corrosion of the reinforcement [11], recycled aggregates in concrete [12], or connector´s strength in steel-concrete composite structures [16]. The effects of ground-granulated blast furnace slag and calcium nitrite-based corrosion inhibitors on the chloride ion permeability and the compressive and tensile strength of concrete specimens have also been adequately modeled using ANN [17]. Köroğlu et al. [18] worked with the flexural capacity of quadrilateral fiber-reinforced polymer confined reinforced concrete columns using both single and combined ANN; the results showed that predictions of the neural simulations were more satisfactory than approaches used currently in the literature. Alshihri et al. [19] satisfactorily modeled the compressive strength of light-weight concrete by using both feed-forward back-propagation and cascade correlation. Madandoust et al. [20] used ANN and adaptive neuro-fuzzy inference to study *in situ* concrete strength by means of cores cut from hardened concrete; the results showed that both methods have great ability for predicting concrete compressive strength. Finally, the split-tensile strength and water permeability of concrete containing Fe_2O_3 nanoparticles was studied by Nazari et al. [21] using ANN and genetic programming. According to their results, both models have strong predicting potential, although ANN exhibited better performance.

The aim of this study is to predict compressive strength of concrete samples containing nS along with SF and/or FA in the presence of SP by using ANN as a tool complementary to a series of DOE at different ages of maturity of the samples. Three different arrays were employed at each age, i.e., DOE I (nS-FA), DOE II (nS-SF), and DOE III (nS-SF-FA). The partition was made in three DOEs keeping in mind that the upper values of each of the variables employed (nS, SF, FA) were developed in the real limits used in field (not only under laboratory conditions). As presented earlier, ANNs have been applied in fields where the development of a theoretical model is not a straightforward task

due to the many parameters involved in the final value of the property being quantified. Consequently, in this research, an ANN approach intends to assist numerical studies on compressive strength based on DOE in order to obtain a better physical understanding of the global behavior of the systems. Contrary to other fields of research where DOE surfaces adjust well [22][23], in cementitious systems sometimes the surfaces exhibit mathematical lack-of-fit (LOF) of the second order [24]. In this investigation, the ANN results were more representative of the surface responses than the results from DOE since the latter exhibited lack-of-fit of the second-order in all of the cases. Consequently, ANN simulations brought forth better understanding of the overall behavior because the evolution through the time of the systems could be captured in a single equation. In addition, the sensitivity analysis conducted on the ANN models helped in understanding the lack-of-fit exhibited by the DOE methodology.

It should be noted that it was not an objective of this paper to develop a comparative study between DOEs and ANNs models. Instead, the goal was to demonstrate the concurrence and complementary roles played by each methodology in evaluating and physically assisting in understanding the complex experimental behaviors found in the concrete sciences. Finally, the novelty in this research consists in mathematical findings by using ANN about the reason why some concrete (cementitious) experiments or models where DOEs are employed exhibit LOF. Numerous papers are focused on either research in cementitious-ANN or cementitious-DOE, while this research is focused on the complementary benefits for concrete research of each one of this powerful techniques. Specifically, a key reason found in this work about the reason why DOEs exhibited LOF is related to the fact that from ANN sensitivity analysis the nS, SF, and FA inputs were not necessarily the most important contributing variables to compressive strength; but nS, SF and FA are often the only inputs in the mathematical DOE analysis. The major importance of these novel findings lies at the moment of making a decision about the pertinence of the most common variables employed in concrete technology in the DOE analysis and their possible relationship with the undesirable but very often LOF, which is exhibited by the majority of the cementitious systems.

2. MATERIALS AND METHODS

2.1 Materials

2.1.1 Portland Cement

The concrete samples were prepared using Portland cement type I according to ASTM C150 [25]. Table 1 shows the physical, chemical, and mineralogical characteristics of the cement. The total amount of alkalis expressed as Na_2O-equivalent was calculated following Ref. [26] and the result was 0.43%.

Table 1. Physical, chemical and mineralogical characteristics of Portland cement.

Constituent	SiO_2	Al_2O_3	Fe_2O_3	CaO	SO_3	MgO	K_2O
(wt%)	20.29	6.40	3.51	65.13	2.65	1.03	0.48
Constituent	Na_2O	P_2O_5	TiO_2	SrO	ZnO	Mn_2O_3	LOI
(wt%)	0.12	0.03	0.26	0.03	0.01	0.06	3.13
Bogue Compounds (wt%)	C_3S=55	C_2S= 16	C_3A=11	C_4AF=11	Physical Characteristics	Blaine 394 (m^2/kg)	Specific Gravity: 2.90

2.1.2 Fine and Coarse Aggregates

The fine aggregate had an SSD specific gravity (SG) of 2.6 and an absorption capacity of 4.1%. Following recommendations for the design of high-strength concrete [27][28], the fineness modulus of the fine aggregate was as coarse as 3.0. The coarse aggregate was crush gravel with a maximum size of 9.5 mm, SG-SSD = 2.7, and absorption capacity of 4.2%. Both materials are in accordance with ASTM C33 [29]. As stated by Almusallam et al. [30] past studies demonstrated that mechanical properties of high-performance concretes are dependent on the quality of the coarse aggregate. Therefore, in the present research, the source of aggregates was the

same for the relatively large number of cylinders employed in the experimental program.

2.1.3 Mineral Admixures

The nS consisted of nanoparticles in the form of opalescent and odorless amorphous silica dispersed in water (slurry). The micro-SiO_2 was conformed to ASTM C1240 [31] and was used in the form of uncondensed dry particles. The class F fly ash that was used was classified as low-calcium ASTM Standard C618 [32] ($SiO_2 + Al_2O_3 + Fe_2O_3 \approx 88\%$). Table 2 shows the principal physical and chemical characteristics of nS, SF, and FA. Fig. 1 shows results of x-ray diffraction (XRD) analysis of FA, SF, and nS powders. The main intensity peaks were associated to 2θ angles of 27°, 22° and 24° for FA, SF and nS, respectively.

Table 2. Principal physical and chemical characteristics of FA, SF and nS.

	FA	SF	nS
	Chemical composition (wt%)		
SiO_2	54.3	91.3	99.9
H_2O	0.7	0.3	---
pH	---	---	9.0
LOI	1.28	---	0.1
	Physical properties		
Specific gravity	2.1	2.3	2.1
Mean size (nm)	25000	200	25
Retained #325 (%)	15.5	---	---
SSA (m^2/kg)	320	25000	109000

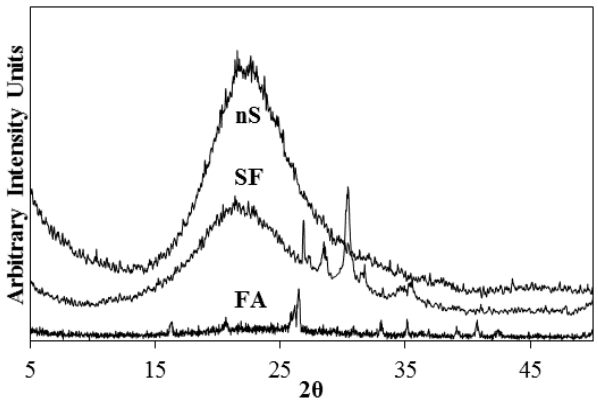

Figure 1. XRD pattern of fly ash and micro/nano-SiO_2 obtained with CuKα radiation.

2.1.4 Chemical Admixture

The SP was a carboxylate-polyether type copolymer conform to ASTM C494 [33] Types A and F and ASTM C1017 [34] type I with SG = 1.08, pH = 4.8-6.8, and 40% of dry active matter. It is commercially designed as a high-range water-reducing admixture (HRWRA).

2.2 Methods

2.2.1 Mix Proportions and Testing Procedures

All the data presented were obtained experimentally by the authors. All the concrete cylinders were cast and cured following the ASTM standard [35], and fractured in the same way in order to attain comparable results. The coarse-to-fine aggregate ratio was 1.50. The cementitious materials' amount was 465±5 kg/m^3 at w/b = 0.35. The concrete constituents were mixed at two speeds i.e., 60 and 120 rpm in a commercial laboratory mixer. The total mixing time was fixed at 5 min. The concrete samples were prepared using the same steps in which 50% of the water and 100% of the fine and coarse materials were mixed for 1.5 min at 120 rpm. Cement was mixed in dry condition with SF (if used) and/or FA (if used), and then this powder mix was added to the mixer for 2 min at 60 rpm. The process was followed by addition of previously mixed remainder water with slurry nS (if used) and the corresponding SP dosage. Thereafter, the materials were mixed for 1.5 min at 120 rpm. The samples were cured in limewater at 23-25 °C. The proper amount of SP had been previously obtained in laboratory experiments for each mix design, higher workability without segregation or excessive bleeding was taken into account. The water content of the SP was accounted in all the mix designs. The fresh concrete was poured into ASTM standard cylinders having 50 mm of diameter and 100 mm in height for testing procedures conforming to ASTM [36]. After pouring and finishing, previously consolidation was carried out by the rodding method. The formwork removal occurred 24 h after casting. The samples were cured in limewater at 23-25 °C until the prescribed period of failure. The mechanical tests were carried out conforming the ASTM procedures for compression tests of the concrete cylinders [37]. Five different ages of testing were conducted in this research: 3, 7, 28, 56, and 90 days of curing using a 3000 kN Forney universal test machine operating in load-controlled setting. Mix proportions and compressive strengths

(Sc) are shown in Table 3.

Table 3. Mix proportions, DOE compositions, and compressive strengths at different ages.

Composition {nS:SF:FA}*	DOE	$\overline{Sc}$ (MPa)**				
		3 days	7 days	28 days	56 days	90 days
{0.0:0.0:0.0}	I-II-III	24.37	31.90	50.30	52.84	54.91
{3.0:0.0:0.0}	I-II-III	36.68	54.06	67.84	70.95	74.81
{6.0:0.0:0.0}	I-II	30.84	51.98	65.13	70.39	73.48
{0.0:0.0:20}	I-III	22.90	29.39	43.70	51.51	54.92
{0.0:0.0:40}	I	13.75	20.29	35.62	43.25	51.65
{3.0:0.0:40}	I	18.74	28.99	40.78	44.90	50.46
{3.0:0.0:20}	I-III	27.58	38.68	52.70	53.91	61.25
{6.0:0.0:40}	I	26.31	36.00	46.19	51.67	58.53
{6.0:0.0:20}	I	35.01	45.04	54.83	60.13	62.36
{0.0:10:0.0}	II-III	26.29	40.84	56.16	59.78	65.42
{0.0:20:0.0}	II	29.02	45.31	63.28	75.09	75.29
{3.0:20:0.0}	II	31.37	46.98	63.36	68.71	76.85
{3.0:10:0.0}	II-III	34.94	47.97	62.72	66.96	70.01
{6.0:20:0.0}	II	36.65	50.89	64.67	71.65	70.63
{6.0:10:0.0}	II	37.64	51.50	60.30	68.29	69.78
{1.5:0.0:10}	III	26.96	37.27	47.97	53.67	55.97
{0.0:10:20}	III	21.08	34.34	48.40	58.74	61.85
{0.0:5.0:10}	III	28.43	37.61	56.99	63.52	65.71
{1.5:5.0:0.0}	III	31.71	44.80	58.14	63.83	63.08
{1.5:10:10}	III	27.10	39.79	56.50	65.44	68.00
{1.5:5.0:10}	III	26.86	39.35	54.57	61.99	64.80
{1.5:5.0:20}	III	22.36	36.56	51.48	57.16	61.97
{3.0:5.0:10}	III	32.67	47.44	59.41	64.09	68.41
{3.0:10:20}	III	24.96	39.92	53.39	59.74	65.46

* Mix proportions are expressed as percentage of cementitious materials. ** The symbol $\overline{Sc}$ stands for average of three replicates.

2.2.2 Development of the ANN and DOE models

In this study, several back-propagation (BP) algorithms were tested in developing the ANN simulations. The BP learning law consists of adjusting the weights and bias values from the output layer toward the input vector by means of an iterative process [38][39]. The target is to minimize the mean squared error (MSE) in each iteration cycle until no further improvement is reached. The general performance of an ANN using BP can be explained as an input vector and a vector bias, at least one hidden layer of neurons, and at least one output (Fig. 2). Mathematically, the functioning of the *n*-th neuron in the *y*-th layer is represented by Eq. (1), where *m* is the number of inputs that arrive at a neuron. A layer of a network includes the combination of the weights (w_{in}), the bias (b_n), the multiplication and summing operations between them, and the transfer function (*f*). The term $p_i^{(y-1)}$ refers to the signal from the *i*-th neuron in the previous layer (*y*-1) that could be the input vector or any hidden layer. The bias term accounts for the parameters whose contribution to the output is either unintentionally missed or cannot be calculated. The vector bias is summed with the weighted inputs to form the net input vector, which is the argument of

the transfer function [40]. This latter function takes the argument and produces the output vector (*o*)(Eq. 1). In the vector input, each neuron receives the variable to be analyzed, whereas the outputs from these first neurons serve as the inputs in the subsequent hidden layers. Finally, the output of the neuron in the last layer is the target that is being sought (Fig. 2).

$$o_n^{(y)} = f\left(b_n^{(y)} + \sum_{i=1}^{m} w_{in}^{(y)} p_i^{(y-1)}\right) \quad (1)$$

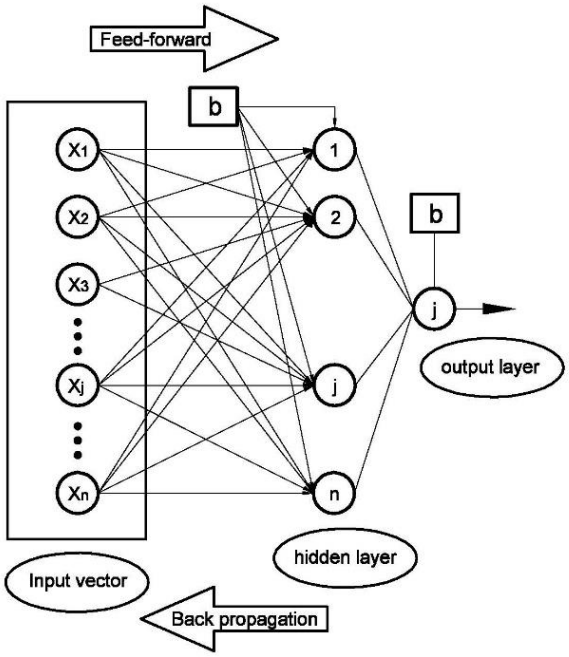

Figure 2. Schematic of a multilayer feed-forward/back-propagation neural network model.

The architecture of a network is the number of layers, the number of neurons, and the type of the transfer function in each layer of a particular network. No unique universal architecture exists; this is a function of each particular problem [15]. Hence, finding the optimum number of neurons in the hidden layer, the number of hidden layers, and the type of transfer function are part of the most complex tasks in ANN simulations [14]. Training the network consists of using a known set of input and output datasets, by means of an iterative process, the optimal set of weight and bias values are reached following a computational algorithm. It is important to note that this algorithm also should be adequately selected to obtain a satisfactory performance of the network. The training process of an ANN can be regarded as solving a complex nonlinear least-square mathematical problem with the difference between the actual and simulated outputs acting as the performance for the problem [41]. In creating an effective network, the training step must be carefully developed because the error surface can converge to a false minimum or to a true minimum but very slowly [10]. Also, the accuracy of the network predictions is strongly related to the selection of the weights in the algorithm [40]. Nevertheless, once the optimum architecture is found, the ANN model is an extremely efficient nonlinear statistical tool for use in complex problems [10][14][15][19][40].

One problem that can occur when training neural networks is that the network over-fits on the training set and does not generalize well to new data [19]. This can be prevented by using computational techniques that usually require a large set of data, which is divided between training and testing sets [42][43][44]. Although the number of data was adequate to perform the DOE methodologies with three replicates and center points, the present study has a relatively limited number of experimental data for the ANN approach. Nevertheless, this was successfully overcome by employing an exhaustive computational preliminary work by testing the convergence of the ANN simulations on several different algorithms, starting from 1 to 20 hidden neurons and from 1 to 2 hidden layers. Also, in view of a certain degree of randomness involved in the development of any ANN model, each one of the trial architectures was studied from at least twenty initial random points in order to avoid false minimum or other local attractors. The separation between training, validation, and testing datasets was: 75%, 5%, and 20% of the total samples data, respectively. The relatively small sample size put an additional challenge to the ANNs that have to be better than 15 DOEs working simultaneously and at the same time the ANN had to show a good generalization capacity. As stated earlier, three independent design of experiments were conducted in the present study for each age of testing (3, 7, 28, 56, and 90 days), referenced hereafter as the following: DOE I consisting of nS(0.0-6.0 wt%)-FA(0.0-40.0 wt%), DOE II consisting of nS(0.0-6.0 wt%)-SF(0.0-20.0 wt%), and DOE III consisting of nS(0.0-3.0 wt%)-SF(0.0-10.0 wt%)-FA(0.0-20.0 wt%). The central composite design models (DOEs I and II) consisted of three replicates with 12 cube points, 3 center points, and 12 axial points with 2

factors (nS/SF, nS/FA). DOE III consisted of three replicates with 24 cube points, 3 center points, and 18 axial points with 3 factors (nS/SF/FA). A total of 27 and 45 runs were conducted randomly within a unit statistical block for DOEs I-II and DOE III, respectively. For all the DOEs, the α-value was set equal to 1 (face-centered). The DOE models were developed in MINITAB® v. 16 statistical software and STATGRAPHICS® CENTURION XV of StatPoint Co. statistical software.

The ranges of the interval values used in each experimental design were selected according to field and literature considerations. The replacement levels commonly employed in the concrete technology industry and related literature are for SF ranges from 5-30 wt% [7][27][45][46]. Replacement levels for FA ranging between 10-40 wt% [5][28][47] are found in field and literature reports, 15 wt% being the usual dosage employed in high-performance concrete [27]. DOE compositions are shown in Table 3. It is important to note that, in the philosophy of the design called High-Volume Fly Ash Concrete (HVFA), the replacements levels of FA (usually Class F) in the mixes normally start at 50 wt% [48][49]. Nevertheless, the designs presented here do not follow the HVFA approach. Additionally, although nS are somewhat new materials in concrete investigations, their most common replacement levels reported in literature and field applications range from 0.5 to 5 wt% [9][24]. For the response variable, the significant terms in the models were found using analysis of variance (ANOVA) and second-order regression analysis. The statistical criterion for factor effect rejection was when their p-values (observed significant level) were greater than 0.05.

In the developing of the ANN-models, all the data points (average of three replicates) of the above DOEs were considered for training, validation, and testing. Many authors [15][38][50][51][52][53] widely recommend that data be normalized before training to prevent extreme numerical values or ranges of any particular parameter from distorting the influence of the other parameters. Hence, the input and output values were normalized (Eq. 2) [52] in the range of [-1, +1] before any numerical simulation were conducted. In the normalization function (Eq. 2), v_i^{norm} and v_i are the normalized and un-normalized values, respectively, of the input/output variables, and v^{min} and v^{max} are the minimum and maximum variable values, respectively.

$$v_i^{norm} = \frac{2(v_i - v^{min}) - (v^{max} - v^{min})}{(v^{max} - v^{min})} \quad (2)$$

In this study, multilayer feed-forward back-propagation neural network is used with a nonlinear logistic sigmoid function (Eq. 3) as the transfer function for the input vector-hidden layer and the identity function as the transfer function for the hidden layer-output layer. The sigmoid activation function is a continuous function often utilized in nonlinear problems because its derivatives can be determined without major computational demand [54]. The ANN was implemented using scripts in MATLAB® v.7.1. During training, the stopping criterion was set to finish when one of the following criteria was met, i.e., the MSE ≤ $1x10^{-4}$, the gradient value was less than $1x10^{-9}$, or the iteration numbers were larger than 1000. In addition to reinforce the accuracy of the architectures, the ANN-simulated outputs were compared with each one of the outputs from the DOEs by mean of the Pearson's correlation coefficient (Eq. 4). In this study, three statistical criteria were selected to compare the ANN simulations results (*Sp*) with the laboratory results (*Sm*) at training, validation, and testing steps, i.e., the root-mean-square error (RMSE) in MPa (Eq. 5), the coefficient of efficiency (CE) (Eq. 6), and the Pearson's correlation coefficient (r) (Eq. 4).

$$f_n^{(y)} = \frac{1}{1+\exp\left[-\left(b_m^{(y)} + \sum_{i=1}^{m} w_{in}^{(y)} o_i^{(y-1)}\right)\right]} \quad (3)$$

$$r = \frac{\sum_{i=1}^{N}(Sm - \overline{Sm})(Sp - \overline{Sp})}{\sqrt{\sum_{i=1}^{N}(Sm - \overline{Sm})^2 \sum_{i=1}^{N}(Sp - \overline{Sp})^2}} \quad (4)$$

$$RMSE = \sqrt{\frac{1}{N}\sum_{i=1}^{N}(Sp - Sm)^2} \quad (5)$$

$$CE = \frac{\sum_{i=1}^{N}(Sm - \overline{Sm})^2 - \sum_{i=1}^{N}(Sm - Sp)^2}{\sum_{i=1}^{N}(Sm - \overline{Sm})^2} \quad (6)$$

$\overline{Sp}$ and $\overline{Sm}$ represent the average of the measured values for compressive strength (MPa) from ANN simulations and laboratory experiments, respectively. *N* is the total number of observations in training, validation, or testing datasets. RMSE has the advantage that larger errors receive much greater

attention than small ones [53]. Pearson's correlation coefficient is a measure of the linear correlation between the ANN simulations and the raw data. In general terms, the correlation values suggest a tendency of the data to plot on a 1:1 straight line when a value tending toward the unit indicates a good linear fit [51]. The coefficient of efficiency is a relative error measure, which in conjunction with RMSE, i.e., a measure of the absolute error, makes the assessment of the models more rigorous [55].

In addition to testing dataset in the ANN models and testing in the DOE statistical softwares, a sensitivity analysis based on the connection weight approach [56] was performed to identify the most important input parameters from the ANN approach. Several different weight and bias values were generated randomly as starting points in order to select the best performance of the trained network parameters. Each one of these random points was checked to meet the aforementioned tolerance stopping criteria. Once the architecture was defined, the actual values of input vector-hidden layer and hidden layer-output layer weights of trained ANN models were used to select the most important input variables following the connection weights and biases procedure, as explained later. A key reason behind the development of the ANN models is related to their potential applicability in conjunction with DOEs. The major importance lies at the moment of making a decision about the pertinence of the most common variables employed in concrete technology in the DOE analysis and their possible relationship with the LOF generally exhibited by some complex cementitious systems.

3. RESULTS AND DATA ANALYSIS

3.1 DOE Analysis

Table 4 shows the compression results from the DOE analysis. In this table, the sign associated with the p-values indicates the positive/negative contribution of each particular term to the strength development. The orthogonality condition was successfully found in all DOEs. The independence, equal-variance, and normality assumptions were carefully checked for each DOE. The linear, interactive, and quadratic regression effects are shown with their associated p-values and Pearson's correlation coefficients. The constant term is not shown due to space considerations but was significant (p-value < 0.05) at all ages and for all designs. The results show the input variables exhibited through the time a variety of p-values, Pearson's values, and linear, interactive, and/or quadratic effects. The continuous changing of the surface responses as the concrete aged (Figs. 3-7) makes the ANN models plausible candidates to be employed as an auxiliary nonlinear statistical tool. Also, the motivation was that all the models showed a LOF of second-order (Table 4). The reader is advised that in Table 4, the DOEs I and II present some empty spaces because SF and FA were not designed input variables for I and II models, respectively. In the development of the second-order polynomial models, the ANOVA results in Table 4 showed that the most important parameters influencing the compressive strength (p-value < 0.05) at all ages were the linear terms of nS and FA and the interactive term nS·SF. Also, the quadratic term of the nS variable (nS·nS) was important for most ages, with minor participation of the quadratic term (SF·SF). The quadratic term of FA (FA·FA) and the interaction between the SF and FA (SF·FA) played a less important role on the strength development in the present study (p-value ≥ 0.05).

It is important to note that the environmental capabilities and the fresh state benefits of the FA motivate the employment of this material in conjunction with nS particles. That is, the FA offers a potential for high replacement levels of cement in a mix design up to 70 wt% [57][58]. Nevertheless, the expected consequence will be a drop in the compressive strength due to the reduced activity of the FA compared to Portland cement, at least at early ages of curing [57][58]. Then, based on the extremely high reactivity capacity of the amorphous nanosilica particles [59][60], the use of nS could be expected to compensate for this negative effect induced by the high FA replacement to Portland cement. Nevertheless, in the present work the statistical results showed that nS particles produced a negative effect on strength development when combined with the FA, as revealed by the nS·FA interactions (p-value < 0.05). Thus, when the FA replacement is at the highest level, i.e., 40 wt% (DOE I), the presence of nS either at the highest (nS = 6.0 wt%) or the lowest level (nS = 0.0 wt%) is not statistically significant at early ages (p-value ≥ 0.05). Only at 90 days does this effect become statistically significant but with negative contribution to strength development. Conversely, at lower FA and nS replacement levels (DOE III), the

interaction effect of these two variables is effectively significant (p-value < 0.05) at all ages. Nevertheless, as in the DOE I, the interaction effect is negative on the strength gain (Figs. 8b-12b).

Table 4. Results of p-values and Pearson's correlation coefficients from DOEs in compression tests.

Age	DOE	nS	SF	FA	nS·SF	nS·FA	SF·FA	nS·nS	SF·SF	FA·FA	LOF	r
	I	0.00(+)	---	0.00(-)	---	0.08(+)	---	0.08(-)	---	0.01(-)	0.00	0.93
3d	II	0.00(+)	0.20(+)	---	0.88(+)	---	---	0.01(-)	0.29(-)	---	0.00	0.88
	III	0.00(+)	0.14(-)	0.00(-)	0.08(-)	0.00(-)	0.07(-)	0.00(+)	0.01(-)	0.01(-)	0.00	0.96
	I	0.00(+)	---	0.00(-)	---	0.23(-)	---	0.00(-)	---	0.70(-)	0.00	0.97
7d	II	0.00(+)	0.28(+)	---	0.00(-)	---	---	0.01(-)	0.95(+)	---	0.00	0.90
	III	0.00(+)	0.00(+)	0.00(-)	0.00(-)	0.00(-)	0.28(+)	0.02(+)	0.00(-)	0.78(-)	0.00	0.97
	I	0.00(+)	---	0.00(-)	---	0.19(-)	---	0.00(-)	---	0.61(+)	0.00	0.97
28d	II	0.00(+)	0.08(+)	---	0.00(-)	---	---	0.00(-)	0.04(+)	---	0.00	0.86
	III	0.00(+)	0.00(+)	0.00(-)	0.00(-)	0.02(-)	0.29(+)	0.00(+)	0.00(-)	0.59(-)	0.00	0.93
	I	0.00(+)	---	0.00(-)	---	0.10(-)	---	0.40(-)	---	0.80(+)	0.01	0.91
56d	II	0.00(+)	0.01(+)	---	0.00(-)	---	---	0.21(-)	0.11(+)	---	0.02	0.81
	III	0.00(+)	0.00(+)	0.00(-)	0.04(-)	0.00(-)	0.09(+)	0.23(+)	0.04(-)	0.18(-)	0.01	0.86
	I	0.00(+)	---	0.00(-)	---	0.02(-)	---	0.08(-)	---	0.48(+)	0.00	0.92
90d	II	0.00(+)	0.00(+)	---	0.00(-)	---	---	0.00(-)	0.03(+)	---	0.00	0.93
	III	0.00(+)	0.00(+)	0.00(-)	0.00(-)	0.01(-)	0.27(+)	0.01(+)	0.06(-)	0.15(-)	0.00	0.89

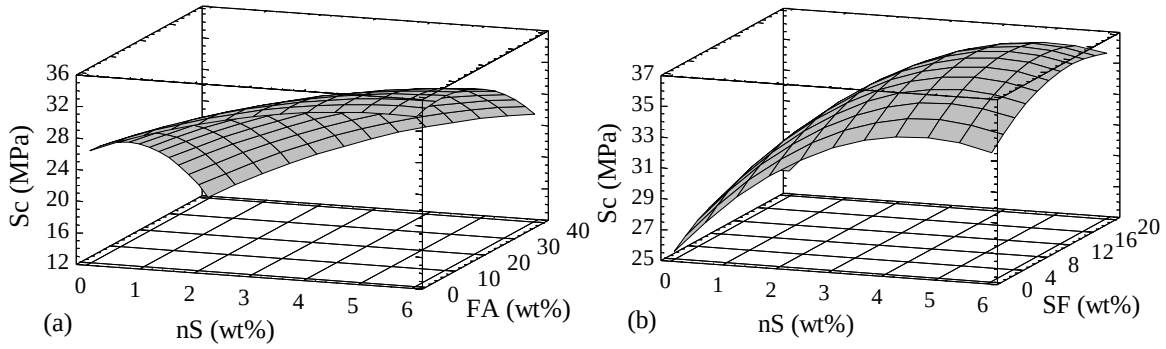

Figure 3. Compressive strength of concretes at 3 days: (a) for DOE I and (b) for DOE II.

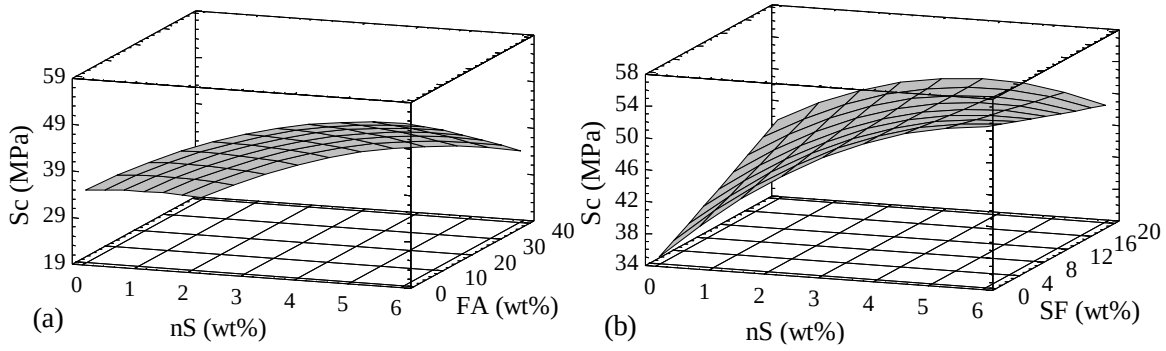

Figure 4. Compressive strength of concretes at 7 days: (a) for DOE I and (b) for DOE II.

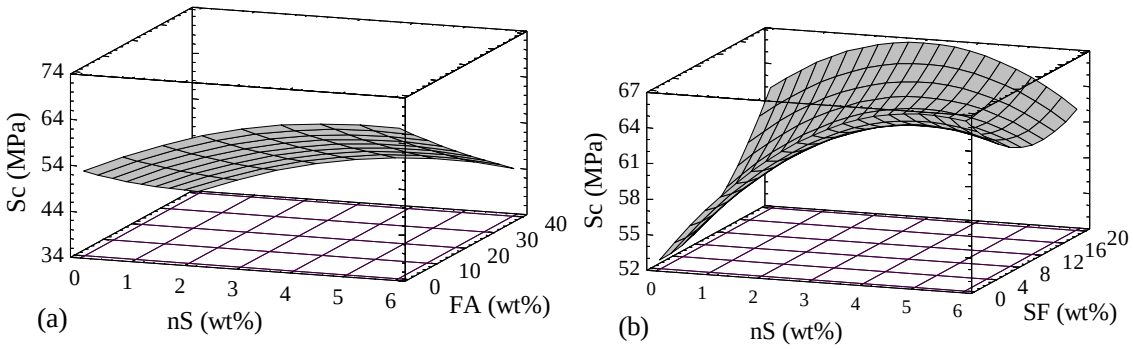

Figure 5. Compressive strength of concretes at 28 days: (a) for DOE I and (b) for DOE II.

Taken into account the FA presence, which usually develops its pozzolanic potential at ages beyond 28 days [27][28][61], in this particular study regardless of the testing time (3 or 90 days) and the nS presence, the FA performance is unclear as can be seen from the experimental results. Also, the quality of the particular FA employed is questionable, as hinted by the morphology in the XRD pattern (Fig. 1) and the amount of noncrystalline silica (Table 2). These observations on the quality of the FA are in agreement with Aïtcin [27] who reported that the FA is one of the most variable and least reactive cementitious materials when compared to slag or SF. At least under the present experimental w/b conditions, age of testing (up to 90 days), and proportions of the combined use of nS and FA, the present results were not favorable. It could be surprising, but a previous research carried out by Kawashima et al. [62] showed that the conjunction use of FA and nS resulted in less pozzolanic activity of the FA after 7 month of maturity. The study demonstrated that due to the presence of 5% nS a double-layer shell structure coated the FA particles, therefore the pozzolanic activity suffered detriment when compared with samples having FA additions but without nS. A similar phenomenon could be present in our research. This is of extreme importance for concrete technology because the nS properties, such as its high surface energy and therefore, its high reactivity capacity could be of interest in mixes with low cement and/or HVFA which are highly FA systems. Nevertheless, more extensive research on the interaction between FA and nS from different sources and at different proportions should be conducted to check this potential harmful phenomenon.

Figs. 3-7 show the strength development through time for DOEs I and II. The surfaces are shown regardless of the p-value. Nevertheless, the analysis in the present study was conducted at the 95% level of confidence. In general terms, it can be noted that, based in the p-value, the most influential linear terms in all models at all ages were the nS and FA contents. The contribution of nS to compressive strength gain is notable while the FA input variable was related to negative influence at all ages. The negative effect of FA is expected at early ages due to the high replacement levels of cementitious material (up to 40 wt%) and the recognized low reactivity of the FA at those early ages [27][57][58]. Nevertheless, the behavior of FA systems was not satisfactory even at ages as long as 90 days (Figs. 3a-7a). The SF had a positive effect being the third statistical ranking linear term in participation on strength development. The statistical significance of the SF variable was noted at 56 days old (Fig. 6b) for high amounts of both nS and SF (DOE II). This could be explained because the extremely high surface energy of the nS particles jeopardized the lower (relative) surface energy of the SF particles, thus its contribution was delayed in the statistical analyses. For small amounts of both nS and SF (DOE III), the SF started to be important at 7 days (Fig. 9b). This latter age is related to the normal rate for the pozzolanic development in SF systems [30].

Laboratory compressive strength values and data from DOEs I and II (Table 4) at all ages exhibited a strong correlation, as reflected by the large r-values [63] (i.e., $r > 0.80$). From a statistical point of view, this represents a good agreement between the model outputs and the experimental results. Nevertheless, the LOF tests revealed that points different from those defined in the inputs cannot be properly represented by the surface generated by the second-

order model. Also, DOE III, which has reduced the highest values of the input variables, induced a change only in the interactive and quadratic effects (Figs. 8-12), altering some answers regarding the DOEs I and II. However, the LOF condition remained unchanged. In addition, by changing the upper limits of the variables in the DOE III, the scatter in the compressive strengths of the systems was larger than in DOEs I and II. This observation takes into account that the Pearson's correlation coefficients were lower in DOE III than in DOEs I and II for all ages, except 3 days.

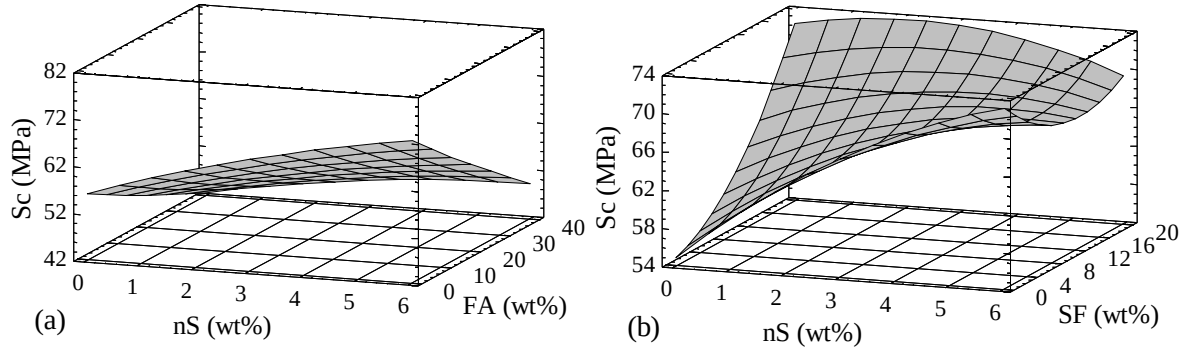

Figure 6. Compressive strength of concretes at 56 days: (a) for DOE I and (b) for DOE II.

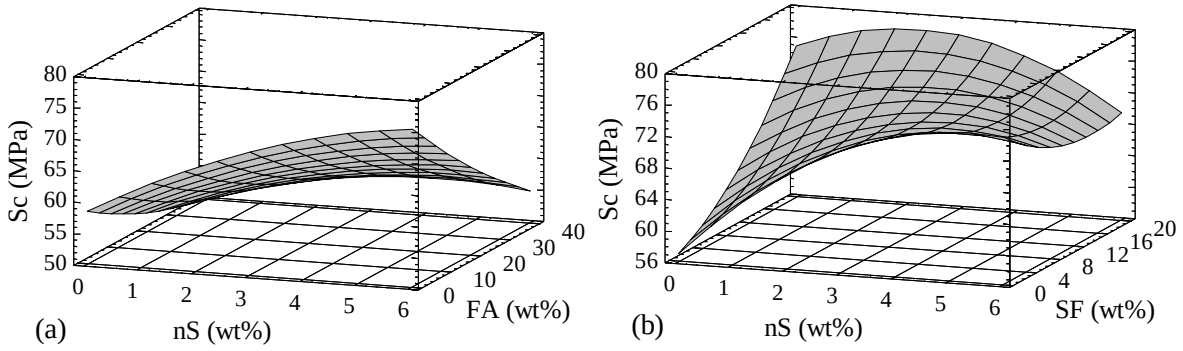

Figure 7. Compressive strength of concretes at 90 days: (a) for DOE I and (b) for DOE II.

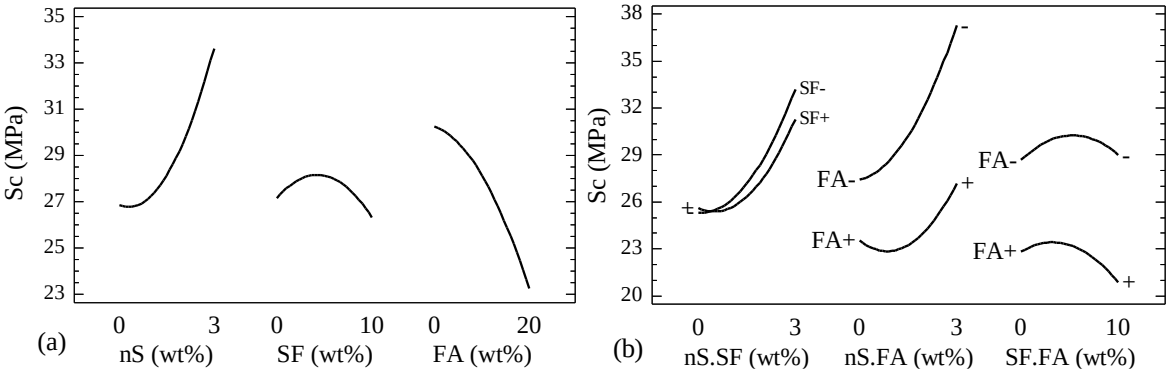

Figure 8. Compression analysis from DOE III at 3 days: (a) principal effects and (b) interactive effects.

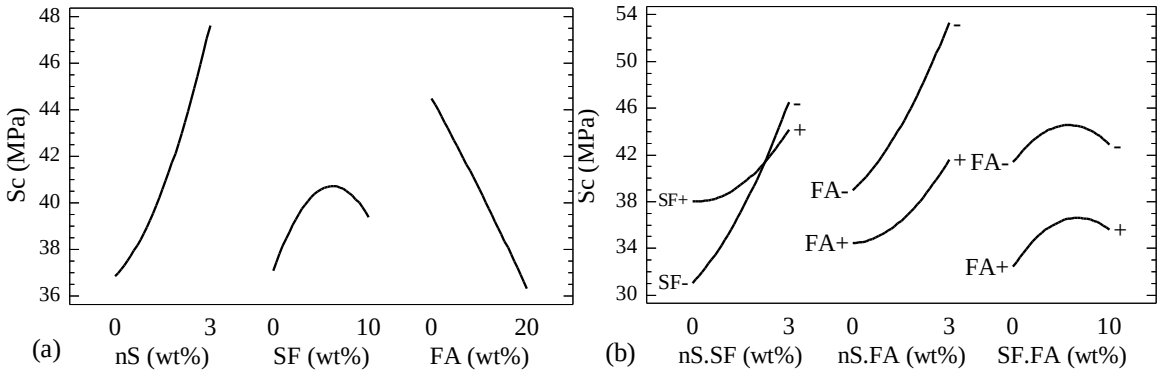

Figure 9. Compression analysis from DOE III at 7 days: (a) principal effects and (b) interactive effects.

The simultaneous incorporation of nS, SF, and FA in the DOE III analysis can be seen in Figs. 8-12. In part (b), the sign of the variable indicates the low (-) or high (+) level of replacement for each one. The surface response for the DOE III in the replacement levels employed here showed statistically significant curvature effects (Table 4 shows the corresponding p-values). These effects are more pronounced as the concrete gained pozzolanic activity, i.e., from 7 days of testing (Figs. 9b-12b). The weighted statistical participation of the nS as principal effect is again noticeable. As for DOEs I and II, the nS presence had a positive effect on strength development. The FA as a linear variable was also significant, but contrarily to nS, FA particles induced a negative effect on strength gain at all ages. Finally, in this segment research, the SF was the least statistically active variable, although its contribution was positive on the strength development. Another important feature regarding the SF additions is that, at higher levels of replacements (DOE II), this variable is active only after 56 days of age. On the other hand, at lower levels of replacements (DOE III), the SF variable is statistically active from the early age of 7 days (Figs. 9a-12a). This can be attributed to more effective particle dispersion at lower dosages.

3.2 ANN Simulations

ANNs are often called “black box” [64][65], but a sensitivity analysis of the bias and weights [20][56][65] in conjunction with another robust statistical tool, such as experiments design, allows the behavior of the parameters to be clarified considerably whereas the prediction models allow a better understanding of the overall complex system behaviors. Since the experimental ranges and/or the input variables were changed in all the DOE analyses and these ranges were taken into account from field values and not only based on laboratory considerations, it can be concluded that changing the experimental intervals is not a plausible option in order to overcome the technical difficulties associated with the LOF in the DOEs. In this sense, the LOF condition is more appropriately interpreted as variance inside the systems additional to the contributions generated by the terms that were considered. Then, the ANN models are expected to help in the understanding of the physical phenomenon by including other input variables in addition to those taken into account in the DOE analysis.

In concrete technology, it is well known that mechanical and durability properties of the concrete depend on the materials’ quality, mix proportions, and the fresh state properties. Regarding fresh state properties, this work proposes considering eight new input variables in order to get more information about the mechanical compression in the hardened state. Also, the maturity age of the concrete had to be considered as an input variable for technical reasons associated with the ANN models. In Table 5, the input variables are nS (nano-SiO_2), SF (micro-SiO_2), FA (Class F fly ash), PC (Portland cement type I), WT (added water), AG (the sum of fine and coarse aggregate contents), SP (superplasticizer), UW (unit weight conforming to ASTM C138 [67], AC (entrapped air content conforming to Ref. [67], FT (flow table test as described in ASTM C1437 [68], IS (initial slump from the slump-cone test conforming to ASTM C143 [69]), and MA (maturity of the concrete at the time of the compression test). The full set of old and new input variables along with their ranges and units are shown in Table 5.

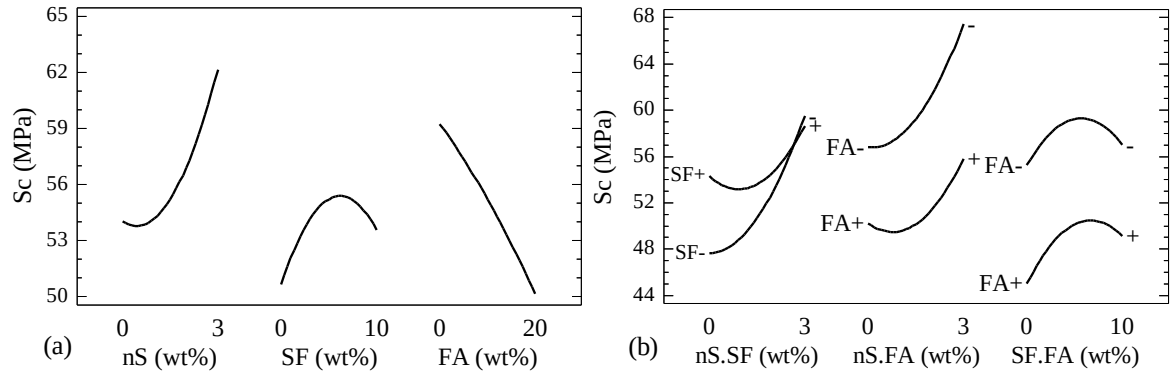

Figure 10. Compression analysis from DOE III at 28 days: (a) principal effects and (b) interactive effects.

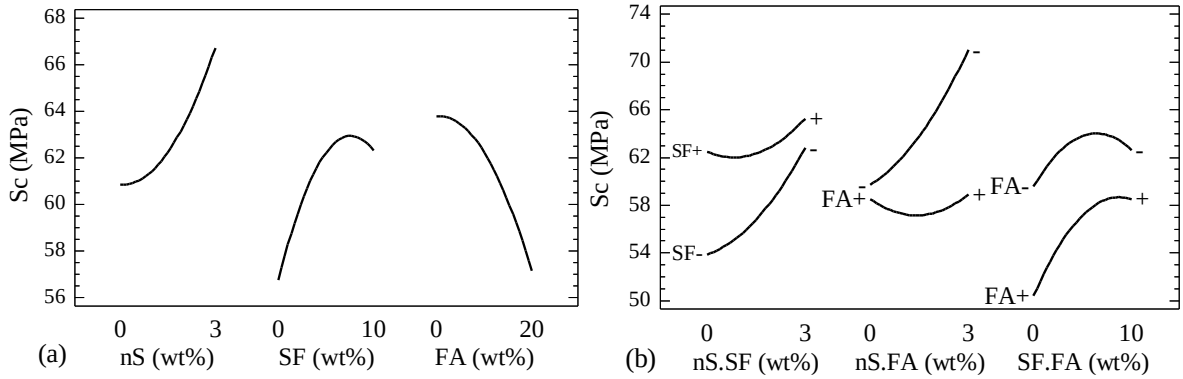

Figure 11. Compression analysis from DOE III at 56 days: (a) principal effects and (b) interactive effects.

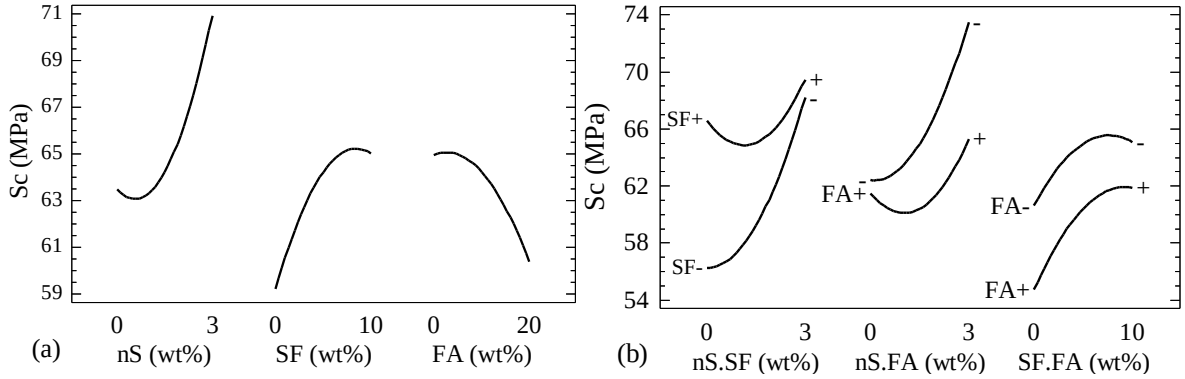

Figure 12. Compression analysis from DOE III at 90 days: (a) principal effects and (b) interactive effects.

All the increment steps of the new input parameters are variable in nature, i.e., none was systematic. In the WT variable, the water contents of the nS (slurry) and the SP were taken into account as well as the absorption requirements by the aggregates. Although the flow table test is employed in cement mortars, in the present study on concrete samples this technique was adopted due to its valuable information on the fresh state in cementitious mixtures. Also, the adoption of the test was reasonable because the maximum aggregate size was 9.5 mm; this means that it is a relatively small particle to be employed in the flow table test. The output of the ANN models is compressive strength (Sc) in MPa, as a function of the mix design components, fresh state properties, and the age at mechanical testing. All the samples were produced, cured, and tested following standard ASTM

protocols in order to obtain an unbiased comparison between and within them. In addition to helping to overcome the LOF condition, ANN simulations are advantageous in providing a single equation to represent all the input variables for the development of the model. In the developing of the ANN models, several simulations were conducted to obtain the response variables using different algorithms and different architectures (arrays) within each algorithm. Also, each algorithm had at least twenty randomly selected initial points for its initialization. In order to find the net´s architectures, the widely used trial-and-error method was employed. Based on the parameters shown in Table 5, back-propagation algorithms (BPA) such as gradient descent with momentum BPA, resilient BPA, Fletcher-Reeves and Polak-Ribiére conjugate gradient BPAs, quasi-Newton BPA, and one-step secant BPA were tested (not shown here). Each of the above BPAs were tested using 1 to 20 hidden neurons, in one and two hidden layers and several values for internal parameters such as learning rate and momentum (values taken from literature). Nevertheless, the performance was not satisfactory because the convergence rate was very slow or the output showed low precision.

Table 5. Design parameters of ANN models.

Variables	Minimum	Maximum	Unit
Inputs			
nS	0.0	28.2	kg/m^3
SF	0.0	93.8	kg/m^3
FA	0.0	187.6	kg/m^3
PC	253.0	469.1	kg/m^3
WT	173.0	220.1	kg/m^3
AG	1585.9	1672.7	kg/m^3
SP	2.8	18.4	kg/m^3
UW	2284.0	2391.0	kg/m^3
AC	3.9	7.1	%
FT	84.0	138.0	%
IS	101.6	130.2	mm
MA	3.0	90.0	days
Output			
Sc	13.8	76.8	MPa

In this study the best performance was obtained by using the Levenberg-Marquardt (LM) BPA. Nevertheless, Bayesian regularization (BR) algorithm (BRA) in combination with early stopping proved to be the most stable and satisfactory algorithm tested. Although no longer required in the BRA, the early stopping was maintained to provide a reasonable basis for comparison among all the algorithms tested. In this sense, the entire algorithms tested had the same number of training (75%), validation (5%) and testing points (20%). These two algorithms, i.e., LMBP and BRA, will be discussed later. In general terms, data for compressive strength using both LMBP and BRA were successfully modeled as compared with the actual data from laboratory experiments. The average results for twelve randomly initial points and internal arrays between training, validation and testing datasets are shown in Table 6. Also, the results from ANN simulations resulted in better performance than results from the fifteen simultaneously DOEs, when compared with the Pearson's correlation coefficients in both aspects as adjusted and predictive models (Tables 7 and 8).

From Table 6, values for RMSE, CE, and r are shown for the best architectures. From this table it is possible to conclude that, in the present work, ANN simulations were suitable computer tools and could adequately predict compressive strength behavior of ternary and quaternary concrete mix designs with values being very close to the actual data. This is in accordance to similar works conducted using ANN or in general intelligent-based modelling methods to predict concrete compressive strength [17][19][20][54][70][71][72][73][74]. For the sake of comparison, Tables 7 and 8 show the Pearson's correlation coefficient values for compression analysis using both DOE methodology and the ANN simulations from the trained networks stated on Table 6. Table 7 shows the r-values for the adjusted models from each DOE, whereas Table 8 shows the r-values from the DOEs as predictive models. For the ANN simulations, each r-value for any particular age of testing was the average of twelve randomly simulations one of which being better than the fifteen r-values from the DOEs. In this work, the requirement imposed on the ANN models was extremely high because in a single equation, the performance of the net is compared against the accuracy of three simultaneous experimental designs conducted at each day of test. With five days of testing and each day having three DOEs, this means that each ANN model had to be better than fifteen

DOEs.

Table 6. Performance of ANN architectures (average of twelve simulations).

ANN Model	Training dataset			Validation dataset			Testing dataset		
	RMSE (MPa)	CE	r	RMSE (MPa)	CE	r	RMSE (MPa)	CE	r
LMBP [12:15:1]	1.578	0.989	0.995	1.499	0.989	0.996	2.384	0.972	0.987
BRA [12:3:1]	1.755	0.987	0.994	1.584	0.989	0.999	2.301	0.974	0.988

Table 7. Results between the adjusted model from DOEs analyses and ANN-models.

DOE	Age (days)	Adjusted r-DOE	Levenberg-Marquardt		Bayesian Regularization	
			r-ANN*	r-ANN/r-DOE	r-ANN*	r-ANN/r-DOE
I	3	0.9341	0.9886	1.0584	0.9842	1.0537
I	7	0.9668	0.9927	1.0268	0.9936	1.0277
I	28	0.9722	0.9789	1.0069	0.9831	1.0112
I	56	0.9100	0.9865	1.0841	0.9874	1.0851
I	90	0.9160	0.9878	1.0784	0.9894	1.0801
II	3	0.8174	0.9800	1.1989	0.9732	1.1906
II	7	0.8954	0.9797	1.0942	0.9837	1.0986
II	28	0.8603	0.9454	1.0989	0.9468	1.1005
II	56	0.8099	0.9673	1.1944	0.9782	1.2078
II	90	0.9271	0.9641	1.0399	0.9761	1.0528
III	3	0.9567	0.9661	1.0098	0.9582	1.0015
III	7	0.9661	0.9793	1.0136	0.9747	1.0089
III	28	0.9246	0.9533	1.0310	0.9513	1.0289
III	56	0.8570	0.9524	1.1113	0.9647	1.1257
III	90	0.8872	0.9489	1.0696	0.9500	1.0708
			average	1.0744	average	1.0763

* Average of twelve simulations.

Table 8. Results between the predictive model from DOEs analyses and ANN-models.

DOE	Age (days)	Predictive r-DOE	Levenberg-Marquardt		Bayesian Regularization	
			r-ANN*	r-ANN/r-DOE	r-ANN*	r-ANN/r-DOE
I	3	0.8901	0.9886	1.1107	0.9842	1.1057
I	7	0.9457	0.9927	1.0497	0.9936	1.0507
I	28	0.9529	0.9789	1.0273	0.9831	1.0317
I	56	0.8407	0.9865	1.1734	0.9874	1.1745
I	90	0.8588	0.9878	1.1502	0.9894	1.1521
II	3	0.6723	0.9800	1.4577	0.9732	1.4476
II	7	0.8243	0.9797	1.1885	0.9837	1.1934

Table 8. Cont.

DOE	Age (days)	Predictive r-DOE	Levenberg-Marquardt		Bayesian Regularization	
			r-ANN*	r-ANN/r-DOE	r-ANN*	r-ANN/r-DOE
II	28	0.7492	0.9454	1.2619	0.9468	1.2637
II	56	0.6384	0.9673	1.5152	0.9782	1.5323
II	90	0.8761	0.9641	1.1004	0.9761	1.1141
III	3	0.9266	0.9661	1.0426	0.9582	1.0341
III	7	0.9409	0.9793	1.0408	0.9747	1.0359
III	28	0.8748	0.9533	1.0897	0.9513	1.0874
III	56	0.7359	0.9524	1.2942	0.9647	1.3109
III	90	0.8046	0.9489	1.1793	0.9500	1.1807
			average	1.1788	average	1.1810

* Average of twelve simulations.

3.2.1 Levenberg-Marquardt Algorithm

Using the LM algorithm twelve input variables and one output neuron were used as fixed numbers and the best architecture consisted of one hidden layer with fifteen hidden neurons (HN); all these parameters are symbolized hereafter as LMBP[12:15:1]. This algorithm was stable only after 13 HN, and the architecture was defined as the smallest number of HN maintaining the RMSE, CE and r-values with high performance in the training, validation, and testing datasets. Also, this architecture was the most stable. Fig. 13 shows a graphical representation of one of the twelve architectures LMBP[12:15:1] of the trained (Fig. 13a) and tested (Fig. 13b) datasets. The values obtained from the trained and tested datasets using ANN simulations are very close to the experimental values obtained in laboratory conditions. The graphical representation for the validation data was omitted due to its small size (5% of the total data), but its global behavior was comparable to the training data (Table 6). In the r-values from DOEs analysis versus LMBP-ANN simulations, the result was satisfactory with all the r-values from the net's architecture being higher than those obtained from DOE analysis (Tables 7 and 8). Also, Table 8 shows the better performance of the ANN simulations as predictive models when compared with the predictive capacity of the DOEs.

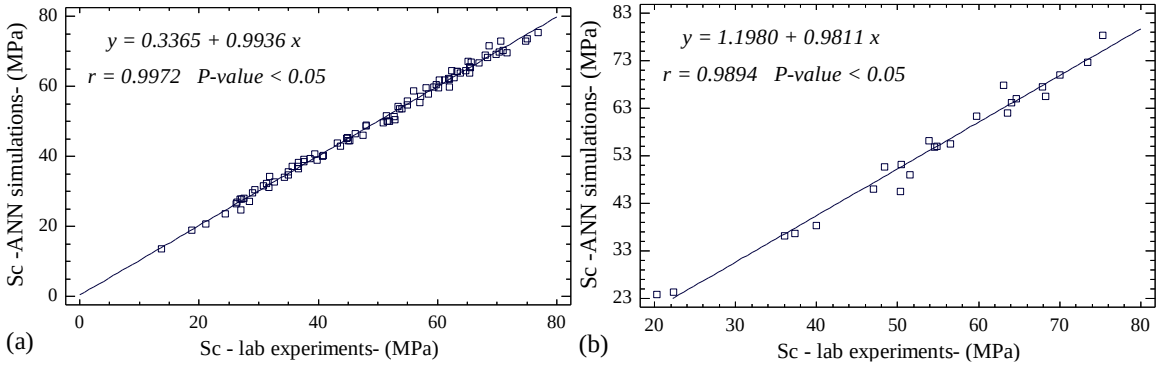

Figure 13. Scatter of actual values of concrete compressive strength and ANN simulated using LMBP[12:15:1] (a) trained dataset (b) tested dataset.

3.2.2 Bayesian Regularization Algorithm

Using the BR algorithm, twelve input variables and one output neuron were set as fixed numbers while the best architecture consisted of one hidden layer with three HN, that is, BRA[12:3:1]. This algorithm was stable from 2 to 9 HN, and the architecture was defined as the smallest number of HN without detriment in the RMSE, CE and r-values in global form (training, validation and testing). Nevertheless, using 4 or 5 HN the precision in training could be improved (not shown here) with insignificant detriment of the validation and testing sets, but the present architecture was defined ([12:3:1]) because of the excellent stability and simplicity. An ANN model of the BRA[12:3:1] architecture is represented in Fig. 14. In the, figure are shown the results of the trained (Fig. 14a) and tested (Fig. 14b) datasets. As in the case for LMBP, the values obtained from the trained and tested datasets using BRA are very close to the actual values. As in LMBP, the graphical representation for the validation data is omitted due to its small size (5% of the total data) being that their overall behavior was better than both the tested and trained datasets (Table 6). With regard to DOEs analysis versus ANN simulations, the results were satisfactory with all the r-values from the BRA being higher than the r-values from DOE analysis (Tables 7 and 8). In a similar fashion, the performance of the BRA was slightly better than the LMBP as compared with the average r-value ratios from Tables 7 and 8, i.e., LMBP(r-ANN/r-DOE) < BRA(r-ANN/r-DOE). Even though the particular run illustrated in Figures 13 and 14 for LMBP and BRA, respectively; seems to show that the precision of the LMBP was higher than the BRA, in general terms (average), the result is the opposite. In this sense, the performance of the LMBP had two principal disadvantages with regard to BRA, i.e., (i) the performance as compared to DOE analysis was slightly inferior (Tables 7 and 8) and (ii) LMBP required a higher number of HN than BRA (Table 6) when the algorithm was stable.

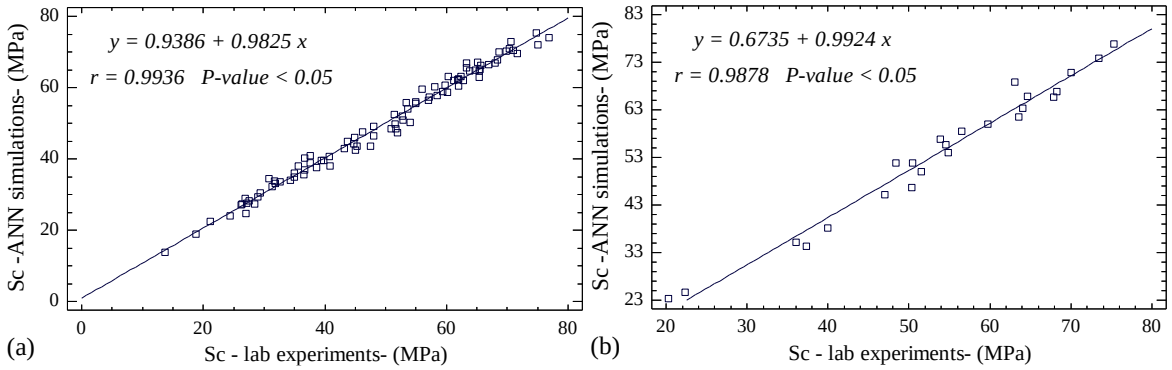

Figure 14. Scatter of actual values of concrete compressive strength and ANN simulated using BRA[12:3:1] (a) trained dataset (b) tested dataset.

3.2.3 Sensitivy Analysis for ANN models

As stated by Lee and Hsiung [65], a sensitivity analysis is required to identify those input variables that are important in contributing to the predicted output variable by each particular ANN model developed. In this study, the sensitivity analysis was based on Ref. [75], which is a connection weights and biases approach. In this method, the actual values of weights and biases between input vector-hidden layers and hidden layers-output layers are considered and the products across all the HN are added [56]. This approach provided explicit numerical (including signs) information on the effect of each input variable on the output. Since the information is presented with the algebraic signs, the connection weight-bias approach permits the analyzer to know if the contribution was directly or inversely related to the output. The relative importance of the input variables related to the output variables is determined using Eq. (7) [76].

$$\beta_i = \frac{\sum_{j=1}^{m} w_{ij} w_{jk}}{\sum_{i=1}^{n} \sum_{j=1}^{m} w_{ij} w_{jk}} \qquad (7)$$

For $i = 1, 2, 3, \ldots, n$; $j = 1, 2, 3, \ldots, m$

In this equation, β_i is the relative importance of *i*-th input variable, *j* is the index number of the HN, W_{ij} is the connection weight between the *i*-th input variable and *j*-th HN, and W_{jk} is the connection weight between the *j*-th HN and the *k*-th output node. Due to the random nature of the initial points of the searching algorithms, the ranking order was established based on the average of twelve simulations. These different arrays included both random initial points and random arrays among the training, validation, and testing datasets. Namely, each trained neural architecture was run from several random conditions, and the connected weights and biases were registered in Table 9. Even so, the net's architecture remained invariant as well as the number of training, validation, and testing points, which were fixed to be 75%, 5% and 20%, respectively, as stated above.

Once the sensitivity analysis was performed for each net's tested architecture, normalization of the numbers based on the highest absolute value was performed. Finally, algebraic summation was carried out in order to rank the relative importance of each input variable (Table 9). Each ranking number is accompanied by the algebraic sign within parentheses after the Arabic number. This easily identifies the nature (directly or inversely) of the relationship between the input and output variables. Regardless of the algebraic sign, when the number increases, the relationship between both variables becomes less significant. Since the input variables are too many (twelve) and based on space considerations, only the contributions from the sensitivity analysis related to the nS, SF, and FA inputs will be analyzed because these variables are common to both the DOE analysis and the ANN simulations. Nonetheless, two controversial points occurred from the ANN analysis.

Table 9. Ranking order for input variables from sensitivity analysis on ANN simulations.

ANN model	nS (kg/m^3)	SF (kg/m^3)	FA (kg/m^3)	PC (kg/m^3)	WT (kg/m^3)	AG (kg/m^3)	SP (kg/m^3)	UW (kg/m^3)	AC (%)	FT (%)	IS (mm)	MA (day)
LM	5(+)	4(-)	2(-)	3(-)	6(+)	11(-)	7(-)	12(+)	10(-)	9(+)	8(-)	1(+)
BR	4(+)	6(-)	3(-)	5(-)	2(+)	12(-)	7(+)	11(+)	9(-)	10(+)	8(-)	1(+)

First, water content (WT) and Portland cement (PC) appeared to produce effects contrary to what one can expect in concrete technology (Table 9). This should be interpreted in relative terms since this study was developed at a fixed w/b = 0.35 with 24 different internal arrays of cementitious mixes (Table 3). It can be explained as follows. At long term, mixes such as {0.0:20:0.0} and {3.0:20:0.0} exhibited higher compressive strengths than the average value obtained by all the systems (Tables 10 and 11). In these mixes with high SF additions, the water requirement is elevated because of the high surface energy of the SF particles. Also, due to the high cement replacement levels, low amounts of PC are required. Therefore, these phenomena were captured by the ANN simulations, and the WT exhibits a positive contribution and the PC a negative contribution. Second, the LMBP revealed that the SP input variable had a negative contribution on compressive strength, whereas BRA exhibited the opposite behavior (Table 9). The SP amounts employed in the mix designs were found in laboratory trials taken into account the maximum capacity of each system (mix design) before segregation or excessive bleeding were seen on any slump-cone or flow table test. However, the excess in SP content could not adversely affect the strength development at neither early nor later ages because the average strength rates for 3d/7d were 0.69 (LM) and 0.73(BR) and for 7d/28d were 0.74(LM) and 0.71(BR), as can be inferred from Tables 10 and 11, which are expected values. Then, from the point of view of concrete technology in systems with mineral additions these values are commonly found. The key point is that the amount of SP supported by FA systems is extremely small before segregation or bleeding is observed as compared to nS-systems. Considering the BRA, the explanation lies in the fact that additions of low calcium FA in the amounts used here (up to 40 wt%) showed good fluidity at the lowest SP contents employed, which is to be commonly expected. Also, from the present laboratory conditions and therefore from ANN simulations, FA-samples developed lower strength

(and strength gain) than plain, SF, and nS systems (Tables 10 and 11), as expected. Therefore, this phenomenon was easily detected by the trained net with architecture BR[12:3:1] showing the SP to be a positive influence on compressive strength. In this respect, ANN analysis by means of the BRA and the actual physical phenomenon agree. In contrast, the result obtained by LMBP algorithm is indicating the opposite behavior; SP increments tend to induce a deleterious effect on the compressive strength (Table 9). This output did not match the experimental conditions found by the authors. We will deal with this topic later in conjunction with the negative sign of the SF input variable captured by both algorithms (Table 9).

All the remaining signs and almost all the positions of the input variables were equally obtained by both algorithms (Table 9). The FA input variable was ranked at the second (LM) and third (BR) positions with negative contributions. This result agreed from DOE analysis (Table 4) where it is classified as significant for all ages and a negative contribution to the strength (p-value = 0.00). From a physical point of view, these results are expected. The nS content was the fourth (BR) and fifth (LM) variable, and its presence is related to compression strength gained. From DOE analysis (Table 4), the nS variable was also related to strength gain (p-value = 0.00); hence the results from ANN are justified. Again, from the concrete technology point of view, these results are expected.

In a similar fashion, the SF input variable was in the fourth (LM) and sixth (BR) ranking in the ANN analysis. This was the most difficult variable to interpret. As can be seen in Table 9, the SF variable was in higher positions (fourth and sixth) indicating a weak effect on strength as compared to nS and FA. This agrees with Table 4 from the DOE methodology where the strength contribution at the ages of 3, 7, and 28 days was not statistically significant (p-value $\geq$ 0.05). This was discussed in an early section of this document. Additionally, taking into account the negative sign, the SF variable contrarily to nS and FA input variables, the results from ANN algorithms do not coincide with the linear terms from the DOE analysis. At this respect, the authors propose two possible explanations: (i) since at early ages, i.e., up to 56 days, the strength rate development of the SF-systems was lower than both plain and nS-systems (Tables 10 and 11), this could be successfully detected by both algorithms. (ii) A more rigorous analysis of DOE analysis (Table 4) reveals that statistically significant higher orders (interactive and quadratic terms) of the SF variable are mostly negative in nature rather than positive, which leads to a deleterious effect on the compressive strength (Table 4). According to the DOE analysis (Table 4), it should be noted, based on the p-value criterion, that the positive linear effect of the SF variable was statistically lesser influential than those observed for the negative nonlinear orders. In this sense, both the BRA and the LMBP showed a negative contribution of the SF on the compressive strength. These results could indicate that these two algorithms adapt better to the negative nonlinear orders of the SF variable rather than the positive linear effect. Nevertheless, while the BRA ranked the SF in the sixth position, the LMBP ranked the SF in the fourth position. Then, for this latter algorithm the role played by the SF variable was more important than that given by BRA. It could be attributed to the large HN present in the LMBP compared to the BRA. That is, the large number of HN in the LMBP tended to capture nonlinearities in the relationship of the variables. This second hypothesis could be also related to the negative behavior of the SP in the LMBP algorithm. From a physical point of view, the authors have reported in other publications [77][78] that a predominant nonlinear effect occurs in the rheological behavior resulting from the simultaneous use of the SP and nS/SF in some cementitious systems.

According to the DOE methodology (Table 4), the LOF condition appeared 100% of the time. This is related to the fact that from ANN sensitivity analysis the nS, SF, and FA inputs were not necessarily the most important contributing variables to compressive strength. LMBP registered the PC input variable as being more significant than SF and nS (Table 9), while BRA showed that the WT input variable was more important than the FA, nS, and SF variables. This analysis takes into account that, in the DOE analysis, the nS, SF, and FA are the only input variables used for the mathematical models. Also, from Table 9 it is seen that the input variable MA (maturity age) had the highest positive contribution in both algorithms. This result is expected because the hydration and pozzolanic reactions are time dependent. Nevertheless, this important (the most significant)

input variable was not considered, since by technical considerations the ANN simulations were conducted using all the data at all ages while the DOE analysis was performed at specific ages of 3, 7, 28, 56, and 90 days. Therefore, for the present experimental and computational research work, it can be argued that statistical analysis in conjunction with ANN simulations with an adequate sensitivity analysis, effectively improved the understanding of the system´s overall behaviors.

Table 10. Comparison of results in compression between actual and simulated values from ANN using LMBP [12:15:1].

Mix proportions* {nS:SF:FA}	3 days Actual	3 days ANN	7 days Actual	7 days ANN	28 days Actual	28 days ANN	56 days Actual	56 days ANN	90 days Actual	90 days ANN
{0.0:0.0:0.0}	24.37	23.52	31.90	34.27	50.30	45.58	52.84	50.46	54.91	55.71
{3.0:0.0:0.0}	36.68	38.26	54.06	53.56	67.84	67.57	70.95	70.26	74.81	72.94
{6.0:0.0:0.0}	30.84	31.61	51.98	49.95	65.13	67.10	70.39	69.88	73.48	72.66
{0.0:0.0:20}	22.90	20.97	29.39	30.55	43.70	42.85	51.51	48.94	54.92	54.71
{0.0:0.0:40}	13.75	13.45	20.29	23.88	35.62	37.19	43.25	43.68	51.65	49.90
{3.0:0.0:40}	18.74	18.90	28.99	28.93	40.78	39.99	44.90	45.27	50.46	51.18
{3.0:0.0:20}	27.58	28.00	38.68	39.37	52.70	51.29	53.91	56.24	61.25	61.68
{6.0:0.0:40}	26.31	26.83	36.00	36.20	46.19	46.37	51.67	51.56	58.53	57.74
{6.0:0.0:20}	35.01	34.59	45.04	44.53	54.83	54.93	60.13	59.49	62.36	64.48
{0.0:10:0.0}	26.29	26.40	40.84	40.22	56.16	56.06	59.78	61.39	65.42	65.67
{0.0:20:0.0}	29.02	29.46	45.31	44.48	63.28	64.15	75.09	73.65	75.29	78.31
{3.0:20:0.0}	31.37	32.20	46.98	45.96	63.36	64.18	68.71	71.61	76.85	75.43
{3.0:10:0.0}	34.94	35.55	47.97	48.65	62.72	62.50	66.96	66.58	70.01	69.99
{6.0:20:0.0}	36.65	36.37	50.89	49.66	64.67	64.92	71.65	69.61	70.63	72.81
{6.0:10:0.0}	37.64	38.44	51.50	49.95	60.30	61.77	68.29	65.56	69.78	69.09
{1.5:0.0:10}	26.96	24.63	37.27	36.58	47.97	48.94	53.67	53.66	55.97	58.61
{0.0:10:20}	21.08	20.63	34.34	34.02	48.40	50.66	58.74	57.13	61.85	62.13
{0.0:5.0:10}	28.43	27.05	37.61	39.17	56.99	55.28	63.52	62.08	65.71	66.90
{1.5:5.0:0.0}	31.71	31.08	44.80	45.15	58.14	59.62	63.83	63.86	63.08	67.78
{1.5:10:10}	27.10	27.75	39.79	38.95	56.50	55.58	65.44	63.82	68.00	68.92
{1.5:5.0:10}	26.86	27.77	39.35	40.76	54.57	54.91	61.99	59.85	64.80	64.41
{1.5:5.0:20}	22.36	24.36	36.56	37.12	51.48	51.58	57.16	57.04	61.97	62.07
{3.0:5.0:10}	32.67	32.69	47.44	45.99	59.41	59.75	64.09	64.09	68.41	68.21
{3.0:10:20}	24.96	25.92	39.92	38.35	53.39	54.14	59.74	60.51	65.46	65.37

* Mix proportions expressed as percentage of cementitious materials.

Table 11. Comparison of results in compression between actual and simulated values from ANN using BRA [12:3:1].

Mix proportions* {nS:SF:FA}	3 days Actual	3 days ANN	7 days Actual	7 days ANN	28 days Actual	28 days ANN	56 days Actual	56 days ANN	90 days Actual	90 days ANN
{0.0:0.0:0.0}	24.37	23.99	31.90	33.13	50.30	46.67	52.84	50.95	54.91	56.10
{3.0:0.0:0.0}	36.68	40.33	54.06	50.33	67.84	65.64	70.95	70.44	74.81	75.41
{6.0:0.0:0.0}	30.84	34.52	51.98	47.36	65.13	67.19	70.39	70.87	73.48	73.90
{0.0:0.0:20}	22.90	21.04	29.39	30.34	43.70	44.80	51.51	50.05	54.92	55.66
{0.0:0.0:40}	13.75	13.85	20.29	23.39	35.62	37.91	43.25	42.84	51.65	48.55
{3.0:0.0:40}	18.74	19.00	28.99	27.41	40.78	40.59	44.90	45.94	50.46	51.81
{3.0:0.0:20}	27.58	28.21	38.68	37.57	52.70	52.01	53.91	56.92	61.25	61.91
{6.0:0.0:40}	26.31	27.27	36.00	35.13	46.19	47.49	51.67	52.56	58.53	57.85
{6.0:0.0:20}	35.01	34.84	45.04	42.38	54.83	54.07	60.13	58.62	62.36	63.18
{0.0:10:0.0}	26.29	27.10	40.84	38.09	56.16	55.09	59.78	59.95	65.42	64.72
{0.0:20:0.0}	29.02	29.35	45.31	43.62	63.28	66.99	75.09	72.05	75.29	76.82
{3.0:20:0.0}	31.37	32.28	46.98	45.24	63.36	65.65	68.71	70.09	76.85	74.07
{3.0:10:0.0}	34.94	36.09	47.97	46.35	62.72	61.98	66.96	66.45	70.01	70.76
{6.0:20:0.0}	36.65	36.86	50.89	48.37	64.67	65.80	71.65	69.61	70.63	72.93
{6.0:10:0.0}	37.64	40.82	51.50	49.81	60.30	63.15	68.29	66.89	69.78	70.33
{1.5:0.0:10}	26.96	24.73	37.27	34.32	47.97	49.07	53.67	54.10	55.97	59.57
{0.0:10:20}	21.08	22.50	34.34	34.05	48.40	51.89	58.74	56.78	61.85	62.19
{0.0:5.0:10}	28.43	27.36	37.61	38.78	56.99	56.53	63.52	61.42	65.71	66.25
{1.5:5.0:0.0}	31.71	33.79	44.80	44.23	58.14	60.14	63.83	64.57	63.08	68.79
{1.5:10:10}	27.10	27.51	39.79	39.62	56.50	58.42	65.44	62.85	68.00	66.86
{1.5:5.0:10}	26.86	28.94	39.35	39.45	54.57	55.62	61.99	60.34	64.80	64.94
{1.5:5.0:20}	22.36	24.69	36.56	35.55	51.48	52.42	57.16	57.43	61.97	62.47
{3.0:5.0:10}	32.67	33.45	47.44	43.49	59.41	58.81	64.09	63.34	68.41	67.73
{3.0:10:20}	24.96	26.70	39.92	38.12	53.39	55.84	59.74	60.60	65.46	65.16

* Mix proportions expressed as percentage of cementitious materials.

4. CONCLUSIONS

The purpose of this study was to analyze the compressive strength of plain, binary, ternary, and quaternary concrete samples containing low calcium fly ash (FA), micro- (SF) and nano-silica (nS) additions in the presence of a superplasticizer (SP). The numerical analyses were conducted using both statistical design of experiments (DOEs) and artificial neural networks (ANNs) methodology. The mechanical properties were analyzed at 3, 7, 28, 56, and 90 days of maturity. The principal results can be summarized as follows:

- The simultaneous used of SF and nS additions in concrete induced a pronounced nonlinear effect on the compressive strength response variable. Also, the curvature exhibited by the response surfaces continuously switched from positive to negative. This complex behavior could induce the lack-of-fit of the second-order model presented in the DOEs with nS, SF, and FA as

inputs. Nevertheless, another explanation on the lack-of-fit can be inferred from the ANN sensitivity analysis, which showed that nS, SF, and FA were not necessarily the most important variables contributing to the compressive strength.

- For compression strength analysis, the replacement of cement by either SF or nS particles could effectively improve the strength gain with respect to the control system. This is attributed to the pozzolanic reaction between the amorphous SiO_2 and the $Ca(OH)_2$ present in hydrated cement. In addition, the higher mechanical performance obtained from the addition of the nano-silica particles compared to silica fume addition was statistically demonstrated by both the DOE analysis and ANN models.
- For the present experimental conditions of w/b, age of testing, quality of FA and proportions, the combined use of nS and FA was not acceptable. Even at the high level of 6.0 wt%, the presence of nS did not compensate for the strength loss induced by the FA additions. All the interactions between the nS with the FA additions exhibited a negative effect as seen in the DOEs. This conclusion is of extreme importance for concrete technology because the properties of nS, such as its high surface energy and therefore, its high reactivity, could be of interest in mixes with low cement and/or low amorphous silica contents that is typical in some systems with high FA additions (i.e., high-volume fly ash concrete). This important phenomenon was correlated with another research carried out on nS and FA [62], where due to the presence of the highly reactive nS particles the pozzolanic effect of FA was jeopardized.
- The trained ANN models were utilized to study the effects of mix proportions of cementitious materials on compressive strength at several ages of testing. The input variables used for the development of the ANN models were the amounts of nS, SF, FA, Portland cement, added water, aggregates and the SP. Also, air content, flow area from the flow table test, initial slump, and the unit weight in the fresh state were used as input variables. From the results, it is possible to conclude that, in the present work, ANN simulations were suitable computer tools and can adequately predict the compressive strength behavior of ternary and quaternary concrete mixes with values being very close to the experimental data.
- The general results from response surface analysis of the design of experiments indicated that, in the developing of the second-order polynomial models, the analysis of variance showed that the most important parameters influencing compressive strength (both positive and negative) were the linear terms of nS and FA and the interaction terms nS•SF and nS•FA. These behaviors were also observed by means of two independent algorithms using ANN simulations.
- In addition to the typical training and testing datasets, the results of the adjusting and predictive capabilities of the ANN models were also compared with those obtained by using fifteen simultaneous designs of experiments through the ages of analysis. In conclusion, excellent performance and good generalization were achieved with the performance of the ANN models being better than that from the design of experiments. Additionally, based on the sensitivity analysis of the ANN models, a physical explanation to the lack-of-fit condition experienced by the design of experiments was provided. In closing, for the present experimental and computational research work, it can be concluded thet DOE methodology in conjunction with ANN simulations and an adequate ANN-sensitivity analysis effectively improved the mathematical and physical understanding of the system's overall behaviors.

5. ACKNOWLEDGEMENTS

The authors would like to thank Engineers (Vicksburg, MS-USA) for insightful advice during the completion of the present research. This material is based upon work supported by the National Science Foundation under grants N° HRD 0833112 and 1345156 (CREST Program). Also, the authors would like to especially thank the Construction Materials laboratory of the Department of Civil Engineering and Surveying at the University of Puerto Rico at Mayagüez campus. Finally, we would like to extend our gratitude to the Geotechnical and Structures Laboratory of the Engineer Research and Development Center, US Army Corps of Engineers, for advice during the

development of the present research. Permission to publish was granted by the Director of the Geotechnical and Structures Laboratory.

6. REFERENCES

[1]. Gopalakrishnan K, Birgisson B, Taylor P, Attoh-Okine NO. (eds.), Nanotechnology in Civil Infrastructure – A Paradigm Shift. Berlin Heidelberg (Germany): Springer-Verlag Ltd., 2011, p. 2-6.

[2]. Dave N, Misra AK, Srivasta A, Sharma AK, Kaushik SK. J. Construction and Building Materials. 2017; 139: 447-457.

[3]. Arora A, Aguayo M, Hansen H, Castro C, Federspiel E, Mobasher B, Neithalath N. J. Cement and Concrete Research. 2018; 103: 179-190.

[4]. Liew KM, Sojobi AO, Zhang LW. J. Construction and Building Materials. 2017; 156: 1063-1095.

[5]. Aïtcin P-C, Mindess S. Sustainability of Concrete. Madison Avenue, New York, NY 10016 (EE.UU): Spon Press Ltd., 2011, Chap. 1.

[6]. Atahan HN, Oktar ON, Taşdemir MA. J. Construction and Building Materials. 2011; 25: 2214-2222.

[7]. Rashid MA, Mansur MA. J. Journal of Civil Engineering IEB. 2009; 37(1): 53-63.

[8]. Bumanis G, Dembovska L, Korjakins A, Bajare D. J. Case Studies in Construction Materials. 2018; 8: 139-149.

[9]. Jalal M, Mansouri E, Sharifipour M, Pouladkhan AR. J. Materials and Design. 2012; 34: 389-400.

[10]. El-Kassas EMA, Mackie RI, El-Sheikh AI. J. Advances in Engineering Software. 2002; 33: 713-719.

[11]. Hendi A, Behravan A, Mostofinejad D, Moshtaghi SM, Rezayi K. J. Construction and Building Materials. 2017; 138: 441-454.

[12]. Paul AC, Panda B, Garg A. J. Measurement. 2018; 115: 64-72.

[13]. Yaman MA, Elaty MA, Taman M. J. Alexandria Engineenring Journal. 2017; 56: 523-532.

[14]. Khanlari GR, Heidari M, Momeni AA, Abdilor Y. J. Engineering Geology. 2012; 131-132: 11-18.

[15]. Arslan MH. J. Advances in Engineering Software. 2010; 41: 946-955.

[16]. Allahyari H, Nikbin IM, Rahimi S, Heidarpour A. J. Engineering Structures. 2018; 157: 235-249.

[17]. Boğa AR, Öztürk M, Topçu İB. J. Composites: Part B. 2013; 45: 688-696.

[18]. Köroğlu MA, Ceylan M, Arslan MH, İlki A. J. Engineering Structures. 2012; 42: 23-32.

[19]. Alshihri M, Azmy AM, El-Bisy M. J. Construction and Building Materials. 2009; 23: 2214-2219.

[20]. Madandoust R, Bungey JH, Ghavidel R. J. Computational Materials Science. 2012; 51: 261-272.

[21]. Nazari A, Riahi S. J. Materials and Design. 2011; 32: 3966-3979.

[22]. Yongfan L, Shuai Z, Jing W. J. Procedia Engineering. 2017; 174: 740-747.

[23]. Chen L, Ma Y, Guo Y, Zhang C, Liang Z, Zhang X. J. Journal of Aerosol Science. 2017; 106: 11-23.

[24]. Senff L, Hotza D, Repette WL, Ferreira VM, Labrincha JA. J. Construction and Building Materials. 2010; 24: 1432-1437.

[25]. ASTM Standard C 150-17, Specification for Portland Cement, West Conshohocken, Pennsylvania, (EE.UU): American Society for Testing and Materials, 2017.

[26]. Mehta PK, Monteiro PJM. Concrete: Microstructure, Properties, and Materials, 3rd Ed. New York (EE.UU): McGraw-Hill Ltd., 2003, p. 209.

[27]. Aïtcin P.-C. High-Performance Concrete. London, (United Kingdom): E & FN SPON Ltd., 1998.

[28]. Caldarone MA. High-Strength Concrete - A Practical Guide, New York (EE.UU): Taylor & Francis Ltd, 2009.

[29]. ASTM Standard C 33-16, Standard Specification for Concrete Aggregate, West Conshohocken, Pennsylvania, (EE.UU): American Society for Testing and Materials, 2016.

[30]. Almusallam AA, Beshr H, Maslehuddin M, Al-Amoudi OSB. J. Cement and Concrete Composites. 2004; 26: 891-900.

[31]. ASTM Standard C 1240-15, Standard Specification for Silica Fume Used in Cementitious Mixtures, West Conshohocken, Pennsylvania, (EE.UU): American Society for Testing and Materials, 2015.

[32]. ASTM Standard C 618-17a, Standard Specification for Coal Fly Ash and Raw or Calcined Natural Pozzolan for Use in Concrete, West Conshohocken, Pennsylvania, (EE.UU): American Society for Testing and Materials, 2017.

[33]. ASTM Standard C 494-17, Specification for Chemical Admixtures for Concrete, West Conshohocken, Pennsylvania, (EE.UU): American Society for Testing and Materials, 2017.

[34]. ASTM Standard C 1017-13, Specification for

Chemical Admixtures for Use in Producing Flowing Concrete, West Conshohocken, Pennsylvania, (EE.UU): American Society for Testing and Materials, 2013.

[35]. ASTM Standard C 192-16a, Standard Practice for making and Curing Concrete Test Specimens in the Laboratory, West Conshohocken, Pennsylvania, (EE.UU): American Society for Testing and Materials, 2016.

[36]. ASTM Standard C 470-15, Standard Specifications for Molds for Forming Concrete Test Cylinders Vertically, West Conshohocken, Pennsylvania, (EE.UU): American Society for Testing and Materials, 2015.

[37]. ASTM Standard C 39-16b, Standard Test Method for Compressive Strength of Cylindrical Concrete Specimens, West Conshohocken, Pennsylvania, (EE.UU): American Society for Testing and Materials, 2016.

[38]. Ince R. J. Engineering Fracture Mechanics. 2004; 71: 2143-2159.

[39]. Fazli HR, Mahdavinejad R. J. Optics and Laser Technology. 2018; 99: 363-373.

[40]. Sidhu G, Bhole SD, Chen DL, Essadiqi E. J. Materials and Design. 2012; 41: 99-107.

[41]. He S, Li J. J. Applied Soft Computing. 2009; 9: 954-961.

[42]. Naderpour H, Rafiean AH, Fakharian P. J. Journal of Building Engineering. 2018; 16: 213-219.

[43]. Golafshani EM, Behnood A. J. Journal of Cleaner Production. 2018; 176: 1163-1176.

[44]. Nikbin IM, Rahimi S, Allahyari H. J. Engineering Fracture Mechanics. 2017; 186: 466-482.

[45]. ACI 363R-92, Report on High-Strength Concrete, Detroit, Michigan, (EE.UU): American Concrete Institute, 1997 with reapproved 1992.

[46]. ACI 234R-06, Guide for the Use of Silica Fume in Concrete. Detroit, Michigan, (EE.UU): American Concrete Institute, 2006.

[47]. Toutanji H, Delatte N, Aggoun S, Duval R, Danson A. J. Cement and Concrete Research. 2004; 34: 311-319.

[48]. Li G. J. Cement and Concrete Research. 2004; 34: 311-319.

[49]. Malhotra VM. J. Concrete International. 2002; 24 (7): 30-34.

[50]. Rafiq MY, Bugmann G, Easterbrook DJ. J. Computers and Structures. 2001; 79 (17): 1541-1552.

[51]. Graham LD, Forbes DR, Smith SD. J. Automation in Construction. 2006; 159: 656-663.

[52]. Zyganitidis I, Stefanidou M, Kalfagiannis N, Logothetidis S. J. Materials Science and Engineering B. 2011; 176: 1580-1584.

[53]. Ashour AF, Alqedra MA. J. Advances in Engineering Software. 2005; 36: 87-97.

[54]. Sarıdemir M, Topcu IB, Özcan F, Severcan MH. J. Construction and Building Materials. 2009; 23: 1279-1286.

[55]. Taormina R, Chau K.-W, Sethi R. J. Engineering Applications of Artificial Intelligence. 2012; 25: 1670-1676.

[56]. Das SK, Basudhar PK. J. Computers and Geotechnics. 2006; 3: 454-459.

[57]. Alghazali HH, Myers J. J. Construction and Building Materials. 2017; 157: 161-171.

[58]. Jiang P, Juang L, Zha J, Song Z. J. Construction and Building Materials. 2017; 144: 677-685.

[59]. Da Silva-Andrade D, da Silva-Rêgo JH, Morais PC, Frías M. J. Construction and Building Materials. 2018; 159: 18-26.

[60]. Xu j, Wang B, Zuo J. J. Cement and Concrete Research. 2017; 81: 1-10.

[61]. Siddique R, Kahn KMI. Supplementary Cementing Materials. Berlin Heidelberg (Germany): Springer-Verlag Ltd., 2011, Chap. 1.

[62]. Kawashima S, Hou P, Corr D, Shah S. J. Cement and Concrete Research. 2013; 36: 8-15.

[63]. Gunaydin O, Gokoglu A, Fener M. J. Advances in Engineering Software. 2010; 41: 1115-1123.

[64]. Arsenovic´ M, Stankovic´ S, Radojevic´ Z, Pezo L. J. Ceramics International. 2013; 39: 2013-2022.

[65]. Lee C-J, Hsiung T-K. J. Computers and Geotechnics. 2009; 36: 1157-1163.

[66]. Guler MO, Artir R. J. Materials and Design. 2007; 28: 112-118.

[67]. ASTM Standard C 138-17a, Standard Test Method for Density (Unit Weight), Yield, and Air Content (Gravimetric) of Concrete, West Conshohocken, Pennsylvania, (EE.UU): American Society for Testing and Materials, 2017.

[68]. ASTM Standard C 1437-15, Standard Test Method for Flow of Hydraulic Cement Mortar, West Conshohocken, Pennsylvania, (EE.UU): American Society for Testing and Materials, 2015.

[69]. ASTM Standard C 143-15a, Standard Test Method for Slump of Hydraulic-Cement Concrete, West Conshohocken, Pennsylvania, (EE.UU): American Society for Testing and Materials, 2015.

[70]. Qi C, Fourie A, Chen Q. J. Construction and Building Materials. 2018; 159: 473-478.

[71]. Vakhshouri B, Nejadi S. J. Neurocomputing.

2018; 280: 13-22.

[72]. Khashman A, Akpinar P. J. Procedia Computer Science. 2017; 108C: 2358-2362.

[73]. Yaseen ZM, Deo RC, Hilal A, Abd AM, Cornejo L, Salcedo-Sanz S, Nehdi ML. J. Advances in Engineering Software. 2018; 115: 112-125.

[74]. Nematzadeh M, Dashti J, Ganjavi B. J. Construction and Building Materials. 2018; 164: 837-849.

[75]. Olden JD, Joy MK, Death RG. J. Ecological modeling. 2004; 178: 389-397.

[76]. Dai X, Huo ZH, Wang H. J. Field Crops Research. 2011; 121: 441-449.

[77]. Zapata L, Molina OI, Portela G, "Rheological behavior between Portland cement type I and commercial silica fume". IN: Proceedings in 13th International congress on the chemistry of cement 2011. Madrid (Spain): ISBN: 84-7292-399-7, 2011, p. 408.

[78]. Zapata LE, Portela G, Suárez OM, Carrasquillo O. J. Construction and Building Materials. 2013; 41: 708-716.